Effect of the Potential of Confined Plasma on End-Loss Ion in GAMMA 10/PDX*)

Seowon JANG, Makoto ICHIMURA, Mafumi HIRATA, Ryuya IKEZOE[1)], Mizuki SAKAMOTO, Shuhei SUMIDA, Koki IZUMI, Atsuto TANAKA, Yushi KUBOTA, Ryo SEKINE, Hiroki KAYANO and Yousuke NAKASHIMA

Plasma Research Center, University of Tsukuba, Tsukuba, Ibaraki 305-8577, Japan
[1)]*Research Institute for Applied Mechanics, Kyushu University, Kasuga, Fukuoka 816-8580, Japan*

(Received 30 September 2018 / Accepted 7 January 2019)

In the GAMMA 10/PDX tandem mirror, studies on divertor physics have been performed in the west end region by utilizing end-loss plasmas flowing from the confinement region. Since the plasma density in the end region is quite low ($\sim 10^{16}\,\mathrm{m}^{-3}$), an increase of the end-loss ion flux is required. The increase of the end-loss ion flux has been obtained by increasing the density in the confinement region on previous experiments. When an additional ICRF heating using the antennas in the anchor cells has been performed, a significant increase of the ion flux has been observed with the increase of the potential in the central cell although the change of line densities in the confinement region is little. The effect of the potential on the ion flux has been examined on the GAMMA 10/PDX using about 10,000 discharges. The ion flux increases almost linearly with the potential and the density increase. By comparing with a simple calculation, the increase of the ion flux is explained by the expansion of loss cone boundary of ions and the decrease of the transport time of the end-loss ions from the confinement region to the end region.

Keywords: mirror confinement, end-loss ion, ion flux, potential, ICRF wave, GAMMA 10/PDX

DOI: 10.1585/pfr.14.2402032

1. Introduction

In linear plasma devices, experiments using end-loss plasmas have been performed for the study of divertor physics in a torus fusion reactor and plasma thrusters for space propulsion [1–5]. In a fusion reactor, high particle flux (10^{23} - $10^{25}\,\mathrm{m}^{-2}\mathrm{s}^{-1}$) and high ion temperature (100 eV) are expected at divertor and scrape-off layer plasmas. To simulate a real reactor environment and progress divertor studies, a control of the end-loss plasmas in linear devices is important.

On GAMMA 10/PDX, studies on divertor physics have been carried out in the west end region by utilizing end-loss plasmas [6, 7]. The temperature of end-loss ions is high enough (over 100 eV) while the density in the end region is quite low ($\sim 10^{16}\,\mathrm{m}^{-3}$). Therefore, it is necessary to increase the density by increasing the particle flux of the end-loss plasma. In previous experiments, ion cyclotron range of frequency (ICRF) heating in the anchor cells has been performed for increasing of the end-loss ion flux [8–11]. A significant increase of the ion flux has been observed with the increase of the plasma potential. In this paper, the effect of the potential of the confined plasmas on the end-loss ion flux is discussed. The experimental setup is introduced in Sec. 2. Experimental results and discussions with a simple calculation are described in Sec. 3 and Sec. 4, respectively. Finally, this paper is summarized in Sec. 5.

2. Experimental Setup

GAMMA 10/PDX is composed of five mirror cells; a central cell, minimum-B anchor cells located on both sides of the central cell, and plug/barrier cells at both ends. Eight sets of ICRF antenna are installed in GAMMA 10/PDX as shown in Fig. 1; two Nagoya Type-III (Type-III) antennas and two double half turn (DHT) antennas in the central cell, three double arc type (DAT) antennas in the anchor cells, and a DHT antenna in the plug/barrier cell. RF systems with five final amplifiers are installed to excite ICRF waves on GAMMA 10/PDX.

In normal discharges, the Type-III antennas in the central cell are used to produce the plasma in the central cell and to heat ions in both anchor cells [12, 13]. The DHT antennas in the central cell are used to excite slow waves and heat ions near the midplane of the central cell. After the initial plasmas are built up with both Type-III and DHT antennas, an additional ICRF heating is performed by using one of ICRF antennas installed in the anchor cells and the plug/barrier cell.

The end-loss ions are measured with end-loss ion energy analyzer (ELIEA) installed at the west end [14, 15].

author's e-mail: jang_seowon@prc.tsukuba.ac.jp

*) This article is based on the presentation at the 12th International Conference on Open Magnetic Systems for Plasma Confinement (OS2018).

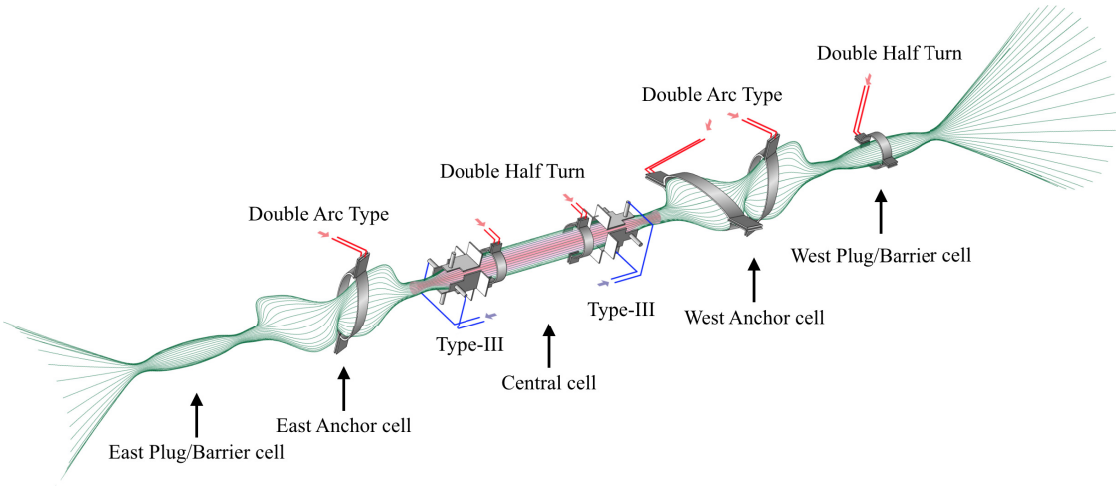

Fig. 1 Schematic drawing of the magnetic field line and ICRF antennas in GAMMA 10/PDX.

ELIEA consists of a slanted ion repeller grid, a secondary electron repeller grid and a collector plate. A positive voltage is applied to the ion repeller grid, and ions reflected by this voltage are collected as the ion current by the collector plate. The energy distribution of the end-loss ions, the end-loss ion flux and the potential of the confined plasma (Φ) are obtained by sweeping the voltage of the ion repeller grid.

3. Experimental Results and Discussions

3.1 Additional ICRF heating with anchor antenna

The additional ICRF wave with a frequency of 7.7 MHz was excited with the DAT antenna installed in the east anchor cell. Since the ion cyclotron frequency in the midplane of the anchor cell is about 9.2 MHz, no ion cyclotron heating occurs with the additional ICRF wave in the anchor cell. Figure 2 (a) shows the diamagnetism in the central cell and the additional ICRF power. Line densities in the central cell and both anchor cells are shown in Fig. 2 (b). The ion flux observed at the west end is plotted in Fig. 2 (c) and the potential of the confined plasma is shown as Fig. 2 (d). The ion flux and the potential are remarkably increased with the additional ICRF heating although the change of the line density is little. The potential measured in the central cell with Gold Neutral Beam Probe also increased with the additional ICRF heating power as same as indicated in Fig. 2 (d).

In the plasma production with the ICRF waves, the plasma density keeps constant due to the eigenmodes formation [16]. Therefore, the plasma production is increased until the density becomes constant and the ion flux increases.

The energy distributions of the end-loss ions are plotted in Fig. 3. Blue and red lines are the measured energy

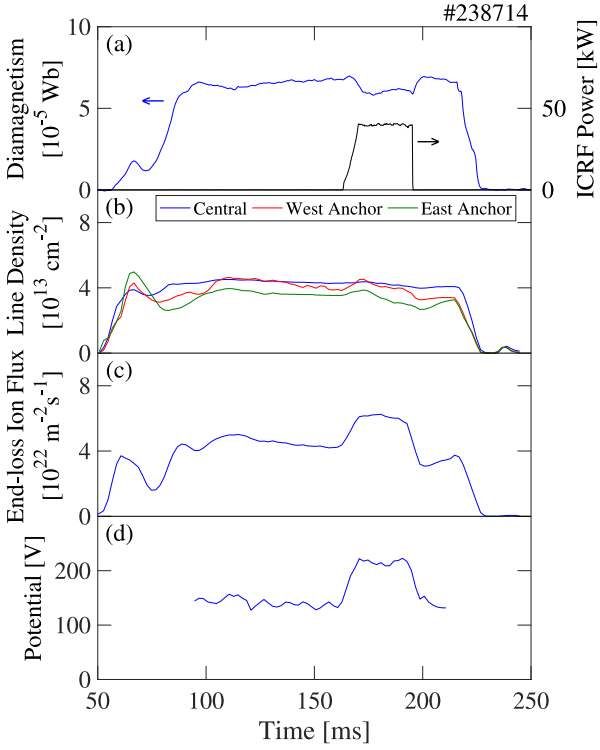

Fig. 2 Time evolution of plasma parameters in the experiment with the anchor antenna.

distributions without the additional heating (135 - 160 ms) and with the additional heating (170 - 195 ms), respectively. The energy distribution shifts from the low energy region to the high energy region with the potential increase. Since the loss cone boundary of ions in the central cell expands with the potential increase, the end-loss ion flux should be enhanced by the potential increase in the confinement region.

The potential increase due to an ICRF wave has been discussed in the previous works [17, 18]. In GAMMA 10/PDX, the mechanism of the increase of the potential

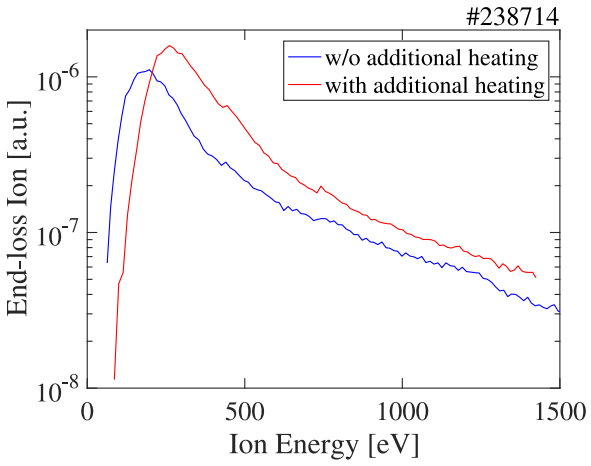

Fig. 3 Energy distribution of the end-loss ions measured in the west end region.

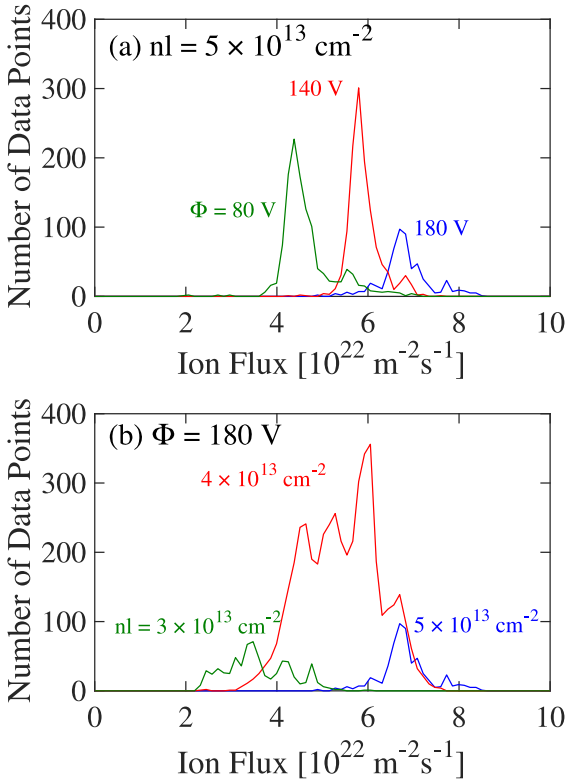

Fig. 4 Number of data points as a function of ion flux.

with the additional heating has not been clarified.

3.2 Qualitative evaluation of effect of the potential

The effect of the potential in the central cell on the end-loss ion flux has been evaluated with discharges from December 2015 to June 2018 (10000 shots) in GAMMA 10/PDX. The discharges in which the end-loss ion flux from the confined region are disturbed by applying the additional heating in the plug/barrier cell and/or obstacles

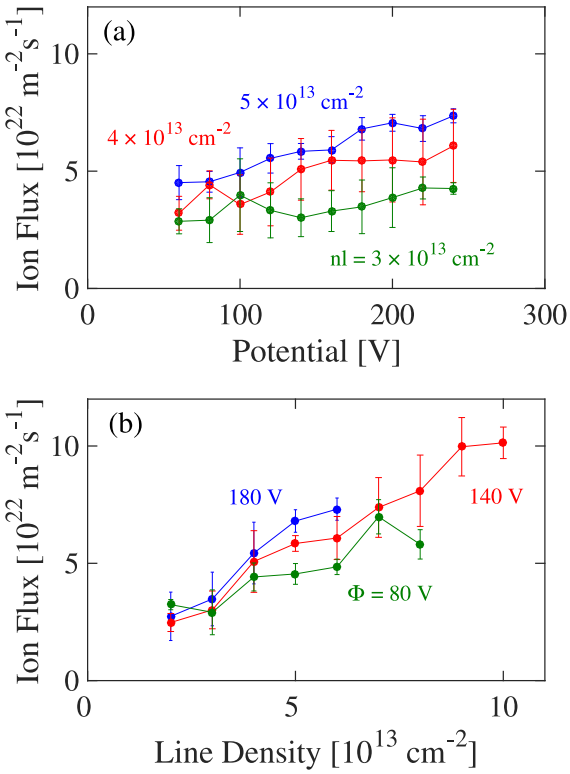

Fig. 5 The ion flux as a function of (a) the potential and (b) the line density.

(for example, probes, divertor simulation module and so on) inserted between confinement region and end region are excluded.

Figure 4 shows the number of data points as a function of the ion flux under (a) the fixed line density of $5 \pm 0.5 \times 10^{13}$ cm^{-2} and (b) the fixed potential of 180 ± 10 V. The values of the line density (*nl*) are averaged values among the line densities in the central and both anchor cells. It is clearly observed that the number of the data points concentrates and form a sharp peak on a certain value of the ion flux when the potential and the line density are fixed. These peaks shift to high ion flux side with increase of the potential and the line density.

Figure 5 shows the ion flux as a function of (a) the potential and (b) the line density under the conditions of the fixed line density and potential, respectively. It is clearly shown that the ion flux increases almost linearly with the increase of the potential and line density.

4. Discussions

In order to investigate the effect of the potential on the end-loss ion flux, orbit of the end-loss ions in one dimensional magnetic field is traced from center of the magnetic mirror configuration to the end region. Collisionless plasma is assumed because the ion-ion collision time is 100 times longer than the average transport time of ions from the central cell to the end region in normal discharges on

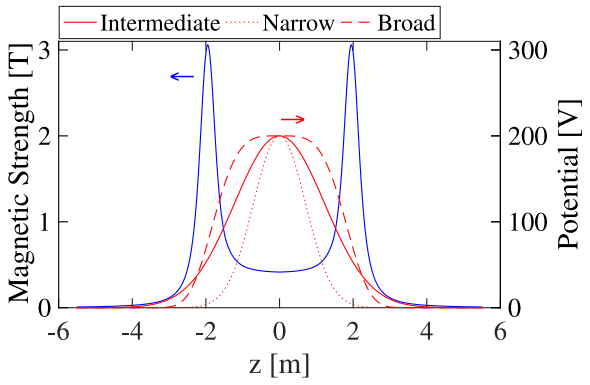

Fig. 6 Magnetic strength (blue line) and potential (red lines) distribution used for calculation. Three types of potential distribution are simulated; narrow type (dotted line), intermediate type (solid line) and broad type (dashed line).

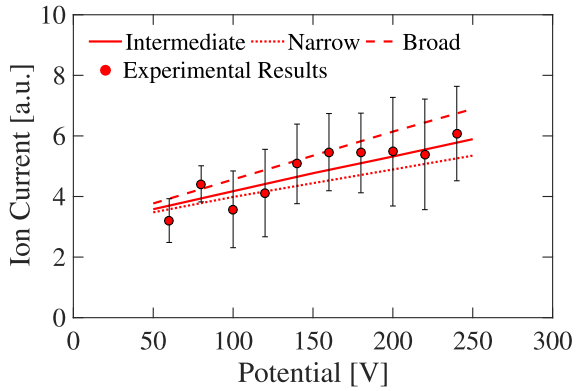

Fig. 7 Potential dependence of the normalized ion current by the calculations. Red circles show the experimental results under the fixed line density of $4 \pm 0.5 \times 10^{13}$ cm^{-2}.

GAMMA 10/PDX. For simplicity, it is assumed that the ions are produced in the center of the mirror and the energy distribution is Maxwellian distribution ($T_{i//} = 300$ eV) with a strong temperature anisotropy ($T_{i\perp}/T_{i//} = 15$) as observed in the experiments. The velocity of the ions is determined by the change of the magnetic field strength and the difference of the potential according to the law of conservation of energy and magnetic moment. The ion current is estimated by dividing the number of the ions by the transport time. Figure 6 shows the magnetic field strength (blue line) and axial potential distributions (red lines) used for the calculations. The increase of the potential is simulated by multiplying the potential distribution. Three types of distributions are simulated; narrow type (dotted line), intermediate type (solid line) and broad type (dashed line). Since the potential measured with ELIEA is almost the same as the potential in the central cell, we used a simple magnetic mirror configuration and peaked potential profile in the at the center.

Normalized ion current of the end-loss ions is plotted in Fig. 7 as red lines as indicated in Fig. 6. The ion current is increased almost linearly with the increase of the potential, which is consistent with the experimental results. The experimental data points in the case of the average line density of $4 \pm 0.5 \times 10^{13}$ cm^{-2} are plotted in the figure. Also, the increase of the ion current is confirmed regardless of the types of the potential distributions as shown in Fig. 7. The number of the end-loss ions is increased by the expansion of the loss cone boundary of ions, and the transport time of the end-loss ions from the confinement region to the end region is decreased by the acceleration of ions due to the potential increase. Furthermore, the density keeps constant since the plasma production increases. Therefore, the ion flux increases with the potential increase.

5. Summary

The effect of the potential on the particle flux of the end-loss ions has been examined on the GAMMA 10/PDX tandem mirror using about 10,000 discharges. The ion flux is almost determined by the potential and the density in the confinement region. It is experimentally confirmed that the ion flux increases almost linearly with the potential and the density increase. It is shown from the comparison with a simple calculation that the observed increase of the end-loss ion flux is explained by the expansion of loss cone boundary and the decrease of the transport time of ions due to the increase of the potential until the plasma production increases.

Acknowledgments

The authors acknowledge the GAMMA 10 group of the University of Tsukuba for their collaboration. This work was partly supported by the bidirectional collaborative research program of the National Institute for Fusion Science, Japan (NIFS14KUGM086 and NIFS17KUGM132).

[1] N. Ohno, Plasma Phys. Control. Fusion **59**, 034007 (2017).
[2] Y. Hayashi *et al.*, Nucl. Fusion **56**, 126006 (2016).
[3] E.A. Bering *et al.*, Adv. Space Res. **42**, 192 (2008).
[4] E.A. Bering III *et al.*, Phys. Plasmas **17**, 043509 (2010).
[5] C.S. Olsen *et al.*, IEEE Trans. Plasma Sci. **43**, 252 (2017).
[6] Y. Nakashima *et al.*, Nucl. Fusion **57**, 116033 (2017).
[7] M. Sakamoto *et al.*, Nuclear Materials and Energy **12**, 1004 (2017)
[8] R. Ikezoe *et al.*, Fusion Sci. Technol. **68**, 63 (2015).
[9] S. Sumida *et al.*, Fusion Sci. Technol. **68**, 136 (2015).
[10] S. Jang *et al.*, AIP Conf. Proc. **1771**, 030011 (2016).
[11] K. Ichimura *et al.*, Plasma Fusion Res. **11**, 2405045 (2016).
[12] M. Inutake *et al.*, Phys. Rev. Lett. **65**, 3397 (1990).
[13] M. Ichimura *et al.*, Nucl. Fusion **28**, 799 (1988).
[14] Y. Sakamoto *et al.*, Rev. Sci. Instrum. **66**, 4928 (1995).
[15] K. Ichimura *et al.*, Plasma Fusion Res. **7**, 2405147 (2012).
[16] Y. Yamaguchi *et al.*, Fusion Sci. Technol. **55**, 106 (2009).
[17] N. Hershkowitz *et al.*, Phys. Rev. Lett. **55**, 947 (1985).
[18] B.A. Nelson and N. Hershkowitz, Phys. Fluids B **4**, 3663 (1992).